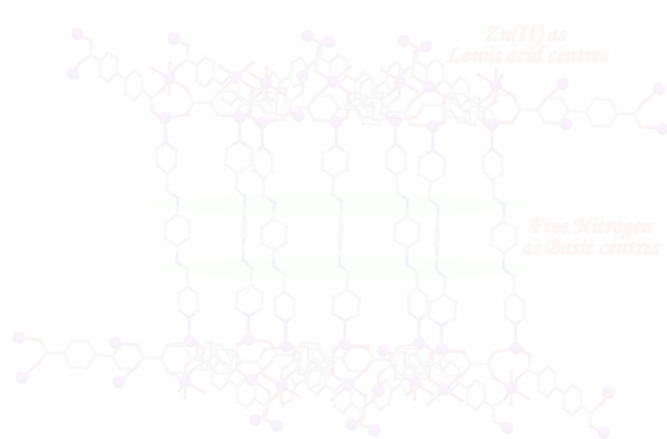


# CHAPTER-7

## Conclusion and Future Scope

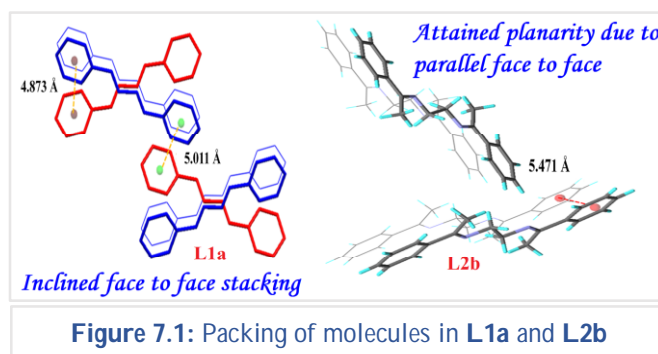


## Conclusion and Future Scope

The current thesis work deals with the crystal engineering studies on imine and amide-based compounds. Bis(pyridyl) imines, bis(pyridyl) amides and bis(pyridyl) sulphonamides were synthesized and some of these compounds were analysed by single crystal XRD. Photophysical properties of the synthesized compounds were explored, and their behaviour was rationalized by understanding their solid-state packing. Coordination polymers of bis(pyridyl) imines and bis(pyridyl) amides were synthesized and networks ranging from 1D to 3D were obtained. The synthesized CPs were explored in various applications such as photocatalytic dye degradation and heterogeneous catalysis for Knoevenagel condensation reaction. The following sections summarize the crux observed in the thesis.

### 7.1 Established the correlation between the crystal packing and photophysical properties of bis(aryl)-di-imines

Chapter 3A, 3B, and 3C describes the photophysical properties of organic compounds. The unique aggregation-induced property of bis(aryl)-di-imines has been discussed in chapter 3A, wherein, the synergistic effect of non-covalent interaction and enhanced



emission of alkylene spacers (ethylene, butylene, and hexylene) in solid-state have been evaluated. Crystal structure analysis of bis(pyridyl)-di-imine rationalised the observed properties. In absence of alkylene in the spacer part, **L1**, showed the formation of H-aggregates and quenching of photoluminescence was observed due to excimer formation. (Figure 7.1) Presence of alkylene spacer also resulted in head-to-head packing or H-aggregation as shown in Figure 7.1, but enhanced emission was observed as the face-to-face stacking of the aromatic groups were prevented due to steric effects of the alkylene spacer groups, which in turn prevented the possibilities of excimer formation or any other non-radiative decay pathways.

Photophysical properties of another category of imines were studied in chapter 3B, where instead of phenyl groups in **L1**, more conjugated luminescent pyrene rings are present, while the spacer groups ranged from alkylene to phenylene. The presence of hydrazine and phenylene in the spacer of these compounds led to ACQ due to  $\pi$ - $\pi$  stacking. Structure emission band was observed in dilute solutions due to reduced  $\pi$ - $\pi$  stacking. Bathochromic shift in UV-visible spectra and crystal structure analysis of phenylene spacer are given to support for appearance

of J-aggregates (Figure 7.2). AIEE was observed when flexible alkylene spacers were present which is attributed to the formation of slipped type of arrangement in the solid state due to the steric considerations of the alkylene group.

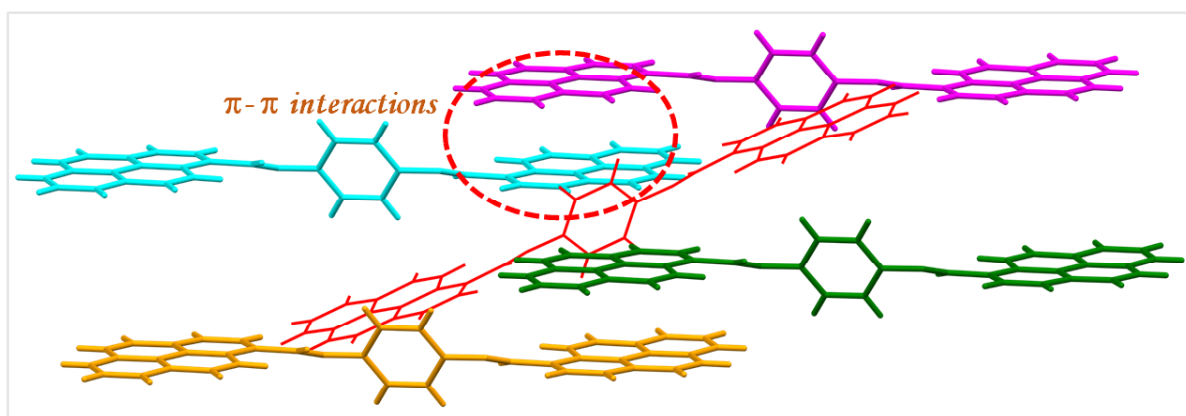


Figure 7.2:  $\pi \cdots \pi$  interactions with head to tail arrangement in **L5a**

A quite different organic linker, bis(pyridyl)-disulfonamides has been explored for photophysical study in chapter 3C. The observed luminescence property was correlated with the non-covalent interactions of crystal packing. The structure of bis(pyridyl)-diamide was compared to understand the geometrical effect in disulfonamides due to the sulfur centre. Here, pyridyl nitrogen position is the main key for turning ACQ to AIE. In bis(pyridyl)-disulfonamides, the position of nitrogen atom in pyridyl ring affected the overall packing and geometry of the molecules which in turn can rationalize the observed photophysical behaviour. Among the compounds studied the chapter, **L10b** was observed to be the most emissive compound due to the formation of a unique non-covalent macrocyclic ring in diluted solution (Figure 7.3). Aromatic stacking of molecules in **L10b** and **L12b** resulted in ACQ which may be due to the excimer formation.

**L11b** showed AIE because the molecules attained a twisting to form a unique non-planar geometry which in turn reduced the aromatic face to face stacking.

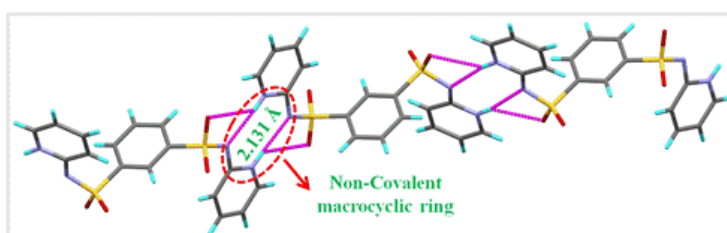


Figure 7.3: Macrocylic chromophore species in **L10b**

## 7.2 Bis(pyridyl)-di-imine as metal-ion sensors

The chelating property of bis(2-pyridyl)-di-imine with several alkali and transition metal ions has been discussed in chapter 4A and 4B. Presence of nitrogen on the pyridyl ring in bis(2-pyridyl)-di-imine favours enhances the possibilities of chelation and in this case, resulted in

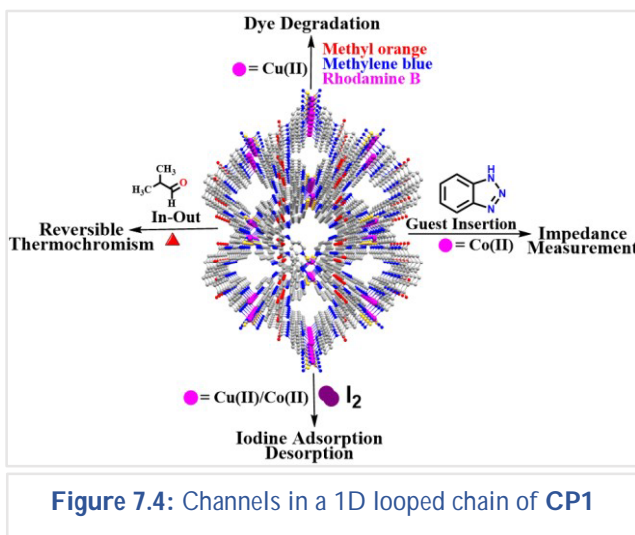
selective binding with metal ion. Suitable pocket size of ligand for metal ion depends on the spacer groups and spacer flexibility which resulted the selective binding of the metal ion through the formation of different sizes of rings.

Chapter 4A describes the effectiveness of **L3c** as a ratiometric chemosensor towards the Ni(II) and Cd(II) ion. Butyl spacer in **L3c** resulted in curved like geometry due to the formation of 5,7,5-membered rings on metal complexation in a 1:1 ratio. The complexation interaction proceeded very fast with micromolar detection level.

In chapter 4B deals the interaction of metal ions with **L2c** and it was proved to be an effective colorimetric fluorescence quencher probe for Fe(II) ion. The interaction study was carried out by UV-visible and emission spectra analysis. In UV-visible region for Fe(II) ion, a distinguished peak corresponding to metal to ligand charge transfer (MLCT) was observed. This was further confirmed by DFT calculations, which inferred that the each molecule of **L2c** was effectively accommodating two Fe(II) ion.

### 7.3 Crystal engineering of 1D looped chain CPs of a 'V'-shaped bis(pyridyl)-diamide: transmetalation reaction, photocatalytic activity, guest exchange and impedance studies

Chapter 5 is based on the synthesis and application of CPs of bis(pyridyl)-diamide, **L15b**, which has a 'V'-shaped geometry. The CP resulted with **L15b** showed a 1D looped chain network, **CP1**. Transmetalation reaction with Cu(II) on the one-dimensional looped chain **CP1** resulted in **CP2**. **CP1** and **CP2** were found to have a band gap of 2.41 eV and 1.30 eV, respectively, and photocatalytic dye



degradation studies showed that **CP2** showed much greater efficiency in degrading the dyes (methylene blue, methyl orange, and rhodamine B) as compared to that of **CP1**. Metal exchange occurred in a single crystal to single crystal fashion with minor geometrical changes. The polar nature of the loops of the chains in **CP1** and **CP2** due to the presence of DMF and it was exploited to study the adsorption and desorption of I<sub>2</sub>. Impedance measurements were also done for **CP1**, **CP2** and guest incorporated **CP1**, and it was observed that benzotriazole incorporated **CP1** showed highest conductivity among them.

## 7.4 Crystal engineering of a 3D metal-organic-framework (MOF) of bis(pyridyl)-di-imine and dicarboxylate linkers: application in Knoevenagel condensation

In chapter 6, detailed structural analysis of a 3D **Zn(II)-MOF** and its catalytic study in Knoevenagel condensation reaction was explored. The **Zn(II)-MOF** formed a 3-fold interpenetrated structure, wherein linear 4,4'-dicarboxylate (**4,4'-bp**) were connected to Zn(II) atom in triangular-tessellated 2D layers and the rigid ligand **L14c** is pillared in a 3D way

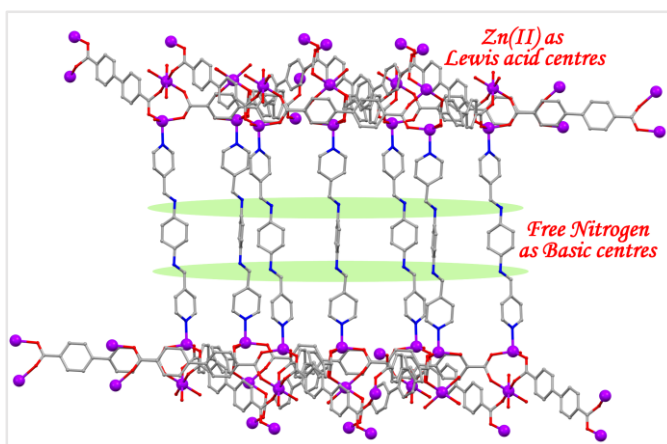


Figure 7.5: Bifunctional acid base centre in Zn-MOF

and resulted in a pinwheel geometry with  $3^6 \cdot 4^{18} \cdot 5^2 \cdot 6^1$  topology. Three such pinwheel networks were interpenetrated and resulted in a narrow pore size channel of  $8.14 \text{ \AA} \times 5.75 \text{ \AA}$ . Two molecules of **L14c** and six molecules of **4,4'-bp** constructed the paddlewheel SBUs which contained Zn-O centres that has acted as Lewis acidic sites for Knoevenagel condensation reaction. **L14c** has provided the basic center for that reaction. Perusing with 5 mg of catalyst loading has given a high yield above 90% within half an hour which was monitored by gas chromatography.

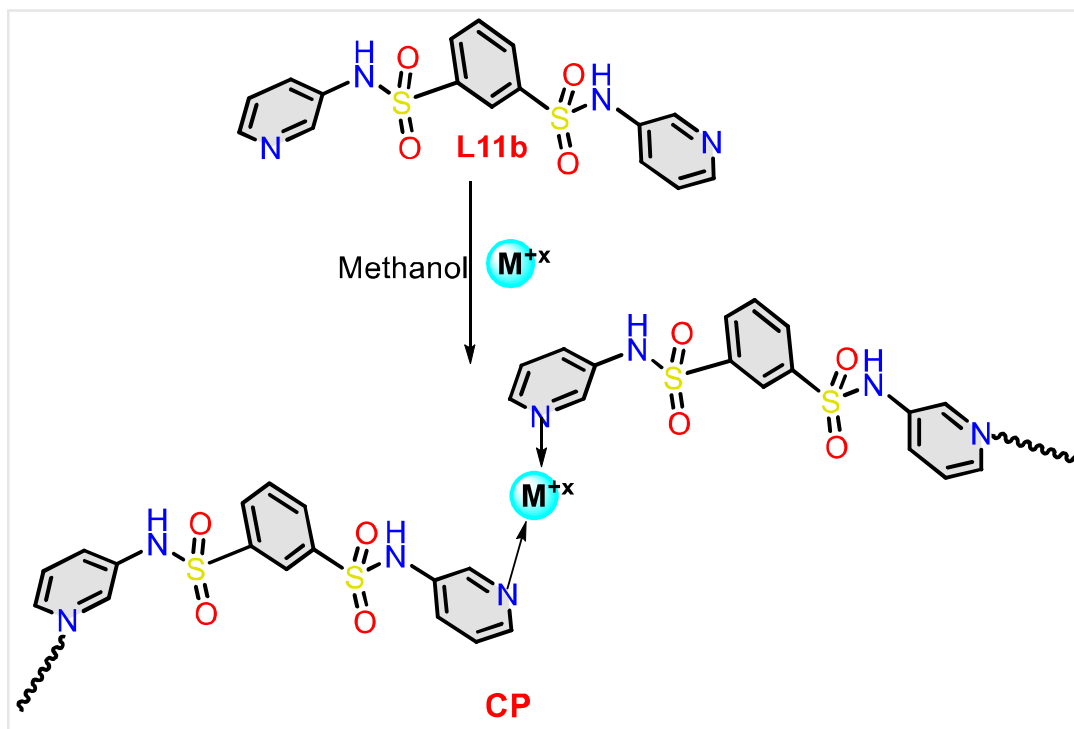
## 7.5 Extension of present work for future outlook

### ✚ Unique photophysical properties of bis(aryl)-di-imine yet to be explored:

In this thesis, photophysical properties of an even number of  $-\text{CH}_2-$  spacer group of bis(aryl)-di-imine in methanolic solution was studied, there is a scope to study the solvatochromism luminescence by varying the odd number of  $-\text{CH}_2-$ /aryl spacer group.

### ✚ CPs/MOFs yet to be explored based on disulfonamide:

In the current work, bis(pyridyl)-disulfonamide (**L10b**, **L11b**, and **L12b**) were synthesized. The disulfonamide is analogous to diamide and contains a hydrogen-bonding synthon and can be explored further in the formation of CPs/MOFs (Scheme 7.1).



Scheme 7.1 Possible CPs from L11b

#### ✚ MOFs of bis(pyridyl)-di-imine/bis(pyridyl)-diamides and their possible applications:

In chapter 6, **Zn(II)-MOF** (Figure 7.6) has resulted in an interpenetrated pinwheel structure constructed by diamine and dicarboxylate ligands and shown a prominent bifunctional catalyst for Knoevenagel condensation reaction. Further, this **Zn(II)-MOF** can be modified by metal ion exchange and can be applied in several catalysis reactions. **Co(II)-MOF** was also synthesized in hydrothermal synthesis as same as **Zn(II)-MOF** and has resulted in pinwheel structure and the **Co(II)-MOF** can be explored in magnetism property. **Zn(II)-MOF** also can be tuned by functionalizing the bis(pyridyl)-di-amide for a better catalytic approach.

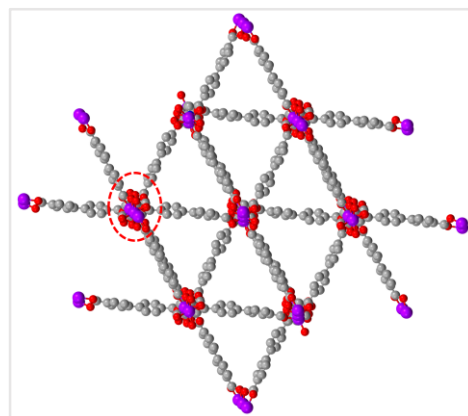


Figure 7.6: Pinwheel structure of Zn(II)-MOF